First measurements at the DAΦNE ϕ-factory with the DEAR experimental setup

M. Augsburger[d], A.M. Bragadireanu[c,f], J.-P. Egger[e], B. Gartner[a], C. Guaraldo[c]
M. Iliescu[c,f], R. King[a], B. Lauss[c,b], C. Petrascu [c,f], J. Zmeskal[a]

[a] *Institute for Medium Energy Physics, Austrian Academy of Sciences,*
Boltzmanngasse 3, A-1090 Vienna, Austria
[b] *on leave from above*
[c] *INFN - Laboratori Nazionali di Frascati, C.P. 13, Via E. Fermi 40,*
I-00044 Frascati , Italy
[d] *Univ. de Fribourg, Inst. de Physique, Bd. de Perolles,*
CH-1700 Fribourg, Switzerland
[e] *Univ. de Neuchâtel, Inst. de Physique, 1 rue A.-L. Breguet,*
CH-2000 Neuchâtel, Switzerland
[f] *on leave from Inst. of Physics and Nuclear Engineering "Horia Hulubei",*
Dept. of High Energy Physics, P.O. Box MG-6 R-76900 Magurele,
Bucharest, Romania

Abstract

The relevant background for the DEAR experiment - low-energy X rays and ionizing particles - present in the DEAR interaction region of the DAΦNE e^+e^- collider was investigated using the first stage DEAR setup and CCD detectors. An extensive Monte Carlo simulation was performed for the present setup and beam conditions. Good quantitative agreement between measurements and simulation was achieved. This is a confirmation that, with respect to the expected background, which gives an important contribution to the statistical precision of the experiment, the configuration chosen to measure the strong interaction shift and width in kaonic hydrogen and kaonic deuterium can indeed reach the planned level of accuracy.

Contents

1 Introduction

A new era in the field of low energy kaon physics will begin with the start of the DAΦNE accelerator at the Frascati National Laboratories (LNF). DAΦNE is a low energy e^+e^- collider (0.51 GeV per beam), with a designed luminosity of $5 \times 10^{32}\ cm^{-2}s^{-1}$ in the 120-bunch mode at a current of 5 A [1], which will deliver kaons with low momentum spread ($\Delta p/p \cong 0.1\ \%$) and high purity (π:K ratio $\cong$ 1:1).

The objective of the DEAR[1] experiment is the determination of the isospin dependent $\bar{\mathrm{K}}\mathrm{N}$ scattering lengths via the measurement of the strong interaction shifts (with a precision of about 1 %) and widths (with a precision of a few percent) of the kaonic hydrogen and for the first time of the kaonic deuterium *K*-series lines [2]. In practice, in the case of kaonic hydrogen, the K_α line is the most important one for the determination of the shift and width of the *1s* level. The detection of the corresponding transition X rays at an energy of approximately 6.15 keV is an inalienable prerequisite.

The main challenge of DEAR is to detect a very weak x-ray signal out of the background of an e^+e^- collider with high statistics and high precision. Previous experiments [3] were unable to detect unambiguously the kaonic hydrogen K_α line, while the experiment which only recently observed these X rays for the first time (KpX at KEK [4]) has only 114 counts in the K_α peak.

In order to overcome the background problem, Charge-Coupled Devices (CCDs) are used as x-ray detectors. CCDs are characterized by a good energy resolution and an unprecedented background rejection capability.

As the huge background was the main limiting factor for all previous experiments, strong efforts have been dedicated to the theoretical study of the expected background at the DAΦNE collider (see in [2]). The work described in this paper had a twofold aim: to understand, on one side, the behaviour of a setup based on CCD detectors used for the first time in the environment of a low-energy and high-current collider such as DAΦNE, and to check the Monte Carlo routines written *ad hoc* to describe the processes involved in a kaonic atom measurement.

The first goal, working in the experimental conditions of a machine in its first stages of commissioning (characterized, in particular, by low injection efficiency and far from optimum vacuum conditions) was reached. The CCD detectors could then be studied at extreme background levels.

The fact that the simulation could reproduce, also quantitatively, the observed features of the interaction region with circulating beams, makes an accurate assessment of the expected background, which principally determines the statistical precision of the exper-

---

[1] DEAR = **DA**Φ**NE E**xotic **A**tom **R**esearch
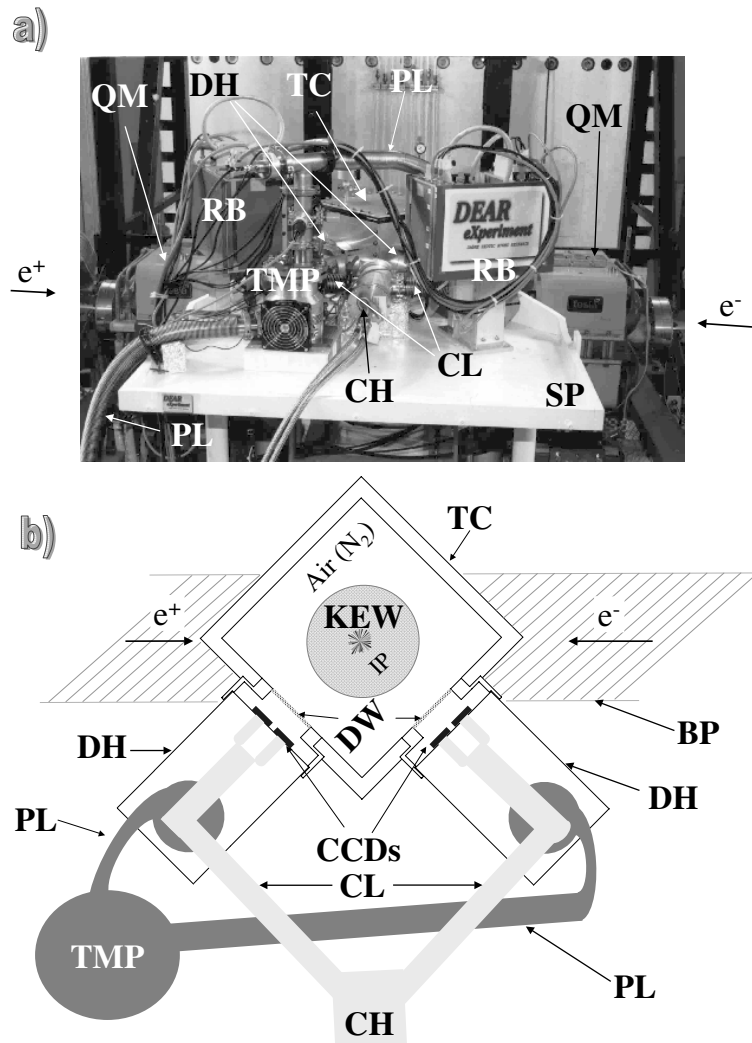
Figure 1: a) The installed NTP setup in the DAΦNE hall as seen from inside the rings. b) Schematic drawing (view from above) of the NTP setup located in the DEAR interaction region above the interaction point in the DAΦNE experimental hall. The setup platform and the magnets of the accelerator are omitted in the drawing for clarity. The displayed components of the experiment are: RB...readout box (CCD electronics), TMP...turbomolecular pump, CH...cooling head, CL...cooling line, PL...pumping line, TC...target chamber, DH...detector housing, QM...quadrupole magnet, BP...beam pipe, KEW...kaon entrance window, DW...detector window, IP...interaction point, SP...setup platform.

iment. With respect to the latter, the measurements therefore demonstrate that the configuration chosen to measure the strong interaction shifts and widths in kaonic hydrogen and kaonic deuterium on DAΦNE can indeed reach the planned level of accuracy [2].

The measurements were performed with the DEAR setup constructed for the detection of kaonic nitrogen lines, which represents the first stage of the experimental program.

2 Experimental setup

The scientific program of DEAR will be developed in two stages: with an NTP[2] target and with a cryogenic target (hydrogen and deuterium).

The NTP target consists of a pure nitrogen volume at room temperature. The purpose is to measure background, compare it to the Monte Carlo calculation, and tune the degrader thickness by optimizing the signal from the kaonic nitrogen transitions $7 \rightarrow 6$ at ~ 4.5 keV and $6 \rightarrow 5$ at ~ 7.5 keV. The yields of these lines are higher (about ten times) than that of the kaonic hydrogen K_α line, so faster feedback is possible. It will be the first measurement of x-rays emitted during the cascade of kaons in nitrogen.

For the measurement of kaonic hydrogen and kaonic deuterium, a pressurized cryogenic gaseous target was developed, to achieve a balance between high kaon stopping in the target cell and decreasing x-ray yield due to Stark mixing. The initial target conditions will be a hydrogen pressure of 3 bar and temperature of 25 K. This will result in a target density of 3.6×10^{-3} g/cm^3 ($\approx 32 \ \rho_{NTP}$). According to cascade calculations [5] and the recent KEK result [4], the expected yield of K_α X rays per stopped kaon in these conditions is (1 - 3 %), depending on the selected values of the cascade parameters.

A photo and a schematical view of the NTP setup used for the measurements discussed in this work is shown in figure 1. The gas volume is a cubic box made of pure aluminum (30 cm x 30 cm x 35 cm), 1.5 cm thick, placed above the specially designed DEAR beam pipe [6] in the DEAR interaction region. The chamber walls are positioned at an angle of 45 degrees with respect to the beam axis. Two CCD detectors with box-shaped housings made of aluminum, each one containing two CCD chips are plugged into two circular openings of the two chamber walls which are on the inner side of the DAΦNE main rings. The CCDs operate in a vacuum of 10^{-5} mbar at a temperature of ~ 170 K. An APD Cryotiger compressor is used to cool the CCDs to the working temperature [7]. Two 50 μm thick Kapton windows separate the CCDs' vacuum from the target chamber, which is filled with nitrogen at NTP or simply air, as in the background measurements. The vacuum of the detector housings is maintained with a turbomolecular pump, placed

---

[2] NTP = Normal Temperature Pressure

3

on the experimental platform and connected, via two ~ 50 cm long tubes, with the detector housings. The vacuum pump is placed on the floor of the experimental area ~ 4 m away.

The target chamber and the CCD detectors were shielded with lead and copper for most of the performed measurements in the following way:

- a layer of lead, 2 cm thick, covered by a layer of copper, 1 cm thick, the latter to shield possible background due to lead fluorescence, were placed beneath the target, having an aperture corresponding to the entrance window of the target cell, which consists of a 190 μm thick Hostaphan and a 100 μm thick aluminum foil. Copper fluorescence was shielded effectively by the thick aluminum target walls and detector housings;

- a layer of lead bricks, 5 cm thick, and a layer of copper, 1 cm thick, were placed on the DEAR platform, all around the target and the detector housings;

- small bags filled with lead shot of ~ 1 mm diameter and with lead powder were placed in all free spaces around the NTP setup;

- a 2 mm thick layer of pure aluminum foil covered the inside of the shielding aperture beneath the kaon entrance window.

The active areas of the detectors were located ~ 142 mm above the beam pipe, at ~ 187 mm vertical distance from the interaction point.

To provide an online energy calibration, pure zirconium (and, for the measurements with the unshielded setup, also pure titanium) foils were put inside the target on the sides, the bottom and the top of the target chamber. For the unshielded setup ~ 600 cm^2 Zr foils and ~ 1000 cm^2 Ti foils were attached; for the shielded setup the Ti foils were removed and further ~ 300 cm^2 Zr foils were added. The remaining inner aluminum surface totalled ~ 3800 cm^2 for the shielded and ~ 3100 cm^2 for the unshielded setup.

3 CCD detectors

The DEAR experiment employs Charge-Coupled Devices (CCDs) as x-ray detectors, which have already been used successfully to investigate X rays originating from exotic atoms [8–10].

The NTP target is equipped with two CCD detectors, each one containing two CCD-05-20-207 chips manufactured by English Electric Valve[3]. Each of these chips has 770 x 1152 ≈ 887000 square shaped pixels, each one of 22.5 μm in sidelength and with a 30 μm de-

---

[3] English Electric Valve (EEV), Waterhouse Lane, Chelmsford, Essex, CM12QU, England.

pletion layer. The chip surface is 17×26 mm$^2 \approx 4.5$ cm^2. The intrinsic x-ray detection efficiency for the CCD-05 chips peaks (85 %) at about 4 keV.

To speed up readout, each chip is electronically split into two halves. The readout of the CCD chip lasts about 64 μs per pixel to guarantee an excellent charge transfer efficiency and therefore a very good energy resolution for X rays. This adds up in total to ∼28 s for the two chips of a detector, which are read in parallel. Up to four chips can be read out simultaneously with the employed electronics. A typical exposure period for the CCDs in the discussed measurements was 10 minutes, after which a CCD "image" was read out. A description of the main features of this special silicon MOS structure detector and readout system can be found in [11–13].

The great advantage of this device for the detection of a weak signal of low-energy X rays in the presence of a huge background consists in its great background rejection capability. This is based on its pixel structure which allows one to apply a selection based on topological and statistical criteria [14].

A selected "single-pixel", that is a pixel with charge content above a selected noise threshold, surrounded by eight neighbour pixels displaying charge contents below that threshold, is considered to be an x-ray hit. This is explained by the fact that a large fraction of the charge created by the interaction of X rays with energies between 1 keV and 20 keV is restricted to the 30 μm thick depletion layer, from where it can be collected by the three electrodes which create one independent potential well which defines a pixel. By far the most important mechanism at these energies is the photoelectric effect.

Hits of more than one pixel are called "clusters" and they are considered to be mainly caused by charged particles traversing the silicon chip and producing by ionization charges also in the bulk material of the chip where these charges can diffuse to neighbouring electrodes and thus create multi-pixel events. Also neutral particles and high-energy γ rays, which are numerously present in the interaction region, can contribute to the amount of clusters due to their production of secondary particles and subsequent electromagnetic cascades.

The employed analysis routines allow us to scan CCD "images", and sort out hits of various cluster sizes. For the present work, only the differentiation between single-pixel events (X rays) and multi-pixel events (clusters) is important.

4 Monte Carlo simulation of the background

The reliability of any simulations depends critically on its performance at very low energies. In particular, the behaviour of photons, electrons and positrons must be accurate below the 10 keV low-energy cut-off of the standard CERN GEANT3 simulation package

[15]. Therefore, a modification of the 3.21 code of GEANT3 [16] was performed. The physical processes in the DAΦNE interaction region and in the DEAR setup which are of interest for the DEAR experiment were simulated, with the aim to optimize the geometry (dimensions, shielding, etc.) and to check the performance (counting rate, background level, etc.).

As far as the signal is concerned, the program generates the primary ϕ mesons produced in e$^+$e$^-$ collisions, taking into account the electron and positron energy spread and beam dimensions in the crossing point. The ϕ mesons are then allowed to decay to all relevant final states according to the known branching ratios.

Decay particles are followed through the experimental setup allowing for energy loss and multiple scattering. They are then allowed to interact both electromagnetically (generating e.m. showers) and hadronically or simply to decay.

An X ray of approximately 6.15 keV is generated for each K^- stopping inside the hydrogen target according to the yield of the $2p \to 1s$ transition [4,5]. X rays are then followed through the setup and registered when arriving on the CCD detectors.

The x-ray background in the region of the signal has two main sources: background generated by ϕ-decay products, among which an important role is played by the hadronic interaction of the stopped K^-. This has been defined as the "hadronic background". The second source is the "machine background", consisting of the products of the electromagnetic cascades generated by the electrons and positrons lost from the primary beams circulating in the rings. One result of the simulation is that the "machine background" is the dominant (98 %) contributor to the total background.

In a low energy machine like DAΦNE, the dominant cause of particle losses is Touschek scattering (elastic Coulomb scattering between two particles within the same bunch). The cross section for this effect is proportional to $1/\gamma^3$, with $\gamma = E/mc^2$. Touschek scattering results in a change of the longitudinal momentum of the two particles: one loses and the other gains the same fraction δ of momentum. If the change exceeds the acceptance of the ring, the particle is lost. All particles which undergo Touschek scattering follow similar trajectories, i.e., with the same betatron oscillation phase and an amplitude proportional to the momentum deviation δ. Since they are in the horizontal plane, in a narrow cone of about 20 mrad, it is possible to reduce this type of background by inserting beam scrapers made by 3.5 mm tungsten - about 10 radiation lengths - upstream of the splitter magnet of each interaction region, to remove the large-amplitude particles. After tracking Touschek scattered particles from the upstream arcs of the ring to the end of the interaction region [17–19], momentum and coordinate distributions were used as input for the DEAR Monte Carlo simulation.

The second source of particle losses is the beam-gas interaction. The two main pro-

cesses which characterize the interaction of the circulating beams of electrons and positrons with the residual gas inside the machine pipe are Coulomb scattering and Bremsstrahlung on gas. A sophisticated simulation of the beam-gas interaction was performed [20] and also used as input for the DEAR Monte Carlo simulation.

During the present work, ϕ-particle production did not occur in the DEAR interaction point and, therefore, the "hadronic background" and eventual background from beam-beam dynamics could not affect the measurements. Accordingly, it was not considered in the simulation. Beam intensity and vacuum conditions were taken from the DAΦNE beam monitor [21].

As the beam scrapers were not closed during the considered measurements, the main part of the background particles was expected to originate from Touschek scattering. This was confirmed by the simulation, which ascribed the main beam losses (~ 80 %) to the Touschek effect. The accuracy of the Monte Carlo simulation was estimated to be about 10 %.

5   Background measurements and comparison with simulation

As seen in the section dedicated to the detector, the two different types of background which affect the CCDs - ionizing particles and soft X rays - appear as cluster events and single-pixel hits, respectively.

Cluster events can be rejected by the employed analysis method but, with an increasing number of hits, the x-ray detection efficiency is decreasing. In other words: the CCDs become "blind". As the CCDs are time-integrating detectors, one should select the exposure time to guarantee only small occupancies[4]. A typical run which still guarantees a good detection efficiency has less than 5 % of all pixels hit. As the readout time cannot be shorter than $\sim$28 s, an evaluation of the overall background is also necessary to determine the level of "blindness" of the CCDs and therefore the exposure time. Consequently, the amount of shielding to allow acceptable working conditions can be deduced as well.

Background X rays cannot be rejected and therefore must be reduced by shielding the setup. They origin in the particles lost from the beams which give rise to e.m. showers whose final products reach the CCDs' surface, or excite the materials of the setup creating electronic X rays. To eliminate the latter, it should be carefully checked that no peak is present in the region of interest of the energy spectrum. The material used for the DEAR target and detector housings was selected to be highly pure (99.99 %) aluminum. Contents of manganese, iron or copper would create very disrupting background lines and severely

---

[4]The occupancy of a CCD detector is defined as the number of pixels which show a hit divided by the total number of pixels.
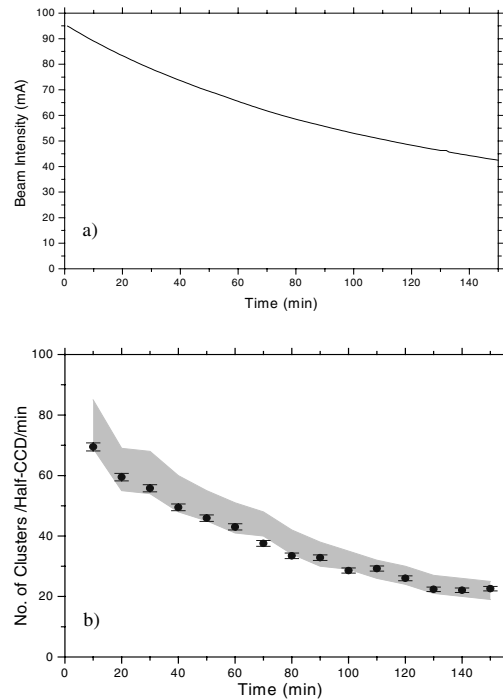
Figure 2: a) Electron beam intensity for the period 0:47 - 3:17 a.m. on June 6, 1999, with only electrons circulating in the DAΦNE main rings, as reported by the DAΦNE beam monitor [21]. b) Observed number of clusters per half-CCD per minute (filled dots) during the corresponding beam period. The shaded area shows the results of the DEAR Monte Carlo simulation.

affect the measurement of the kaonic hydrogen X rays. Background X rays come as well from the non-machine (in the absence of any beam) background, i.e. cosmic rays, natural radioactivity present in the volcanic rocks of Castelli Romani region, where Frascati is located, etc.

Finally, one should mention that depending on the energy of the X ray and on the thickness of the CCDs' depletion layer, soft X rays may also create multi-pixel, mostly double-pixel, hits [22].

The following types of beams were monitored in the period from March to July 1999:
i) only electron beam,
ii) only positron beam, and
iii) electron and positron beams at the same time, but separated in the DEAR interaction region.
Most of the measurements were performed with full shielding.
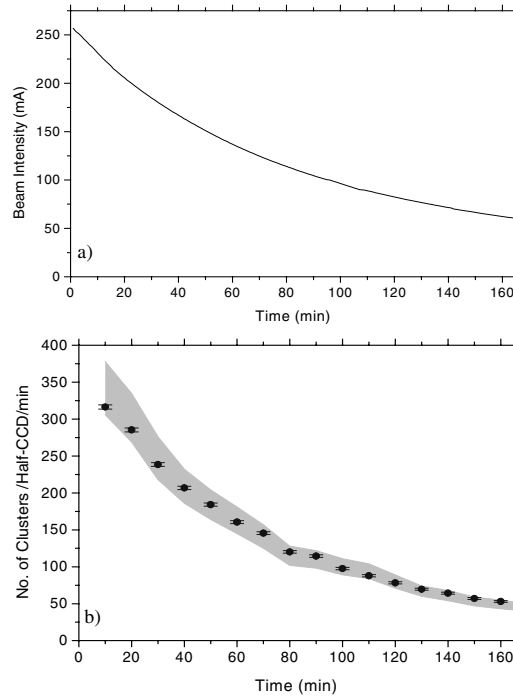
Figure 3: a) Electron beam intensity (mA) for the period 6:21 - 9:01 a.m. on June 27, 1999, with only electrons circulating in the DAΦNE main rings, as reported by the DAΦNE beam monitor [21]. b) Observed number of clusters per half-CCD per minute (filled circles) during the corresponding beam period. The shaded area shows the results of the DEAR Monte Carlo simulation.

5.1 Cluster observation

A quantitative measurement of the beam-induced background was obtained by observing the number of clusters created in the CCD chips.

The given numbers of clusters have been corrected for the non-machine background. In a period without beams in DAΦNE, measurements of the non-machine background rate with the installed NTP setup were performed [23,24]. The corresponding rates were found to be:

$\sim$ 3.8 clusters/half-CCD/min for the setup without shielding,

$\sim$ 2.7 clusters/half-CCD/min for the setup with shielding.

Preliminary background studies - with only one CCD detector, without target cell, and the configuration of the interaction region adopted for machine commissioning ("Day-One") - were done during the first beams circulating in DAΦNE [25,23].

During all the measurements, simulations have been used to improve the detector

performance [26–28].

5.1.1 Background from circulating beams

In the following, some examples of the performed measurements and their comparison with the DEAR Monte Carlo simulation are given. The simulation took into account beam intensity, beam lifetime and vacuum conditions. The average vacuum of the DAΦNE main rings in the considered beam periods was between 10^{-8} and 10^{-9} mbar, mainly depending on beam intensities.
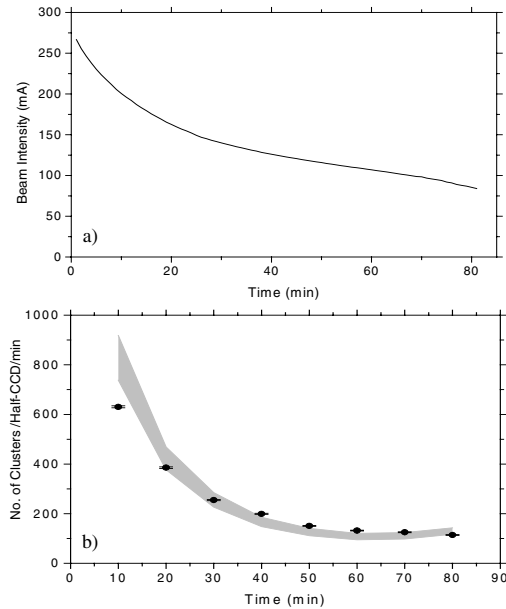
Figure 4: a) Positron beam intensity for the period 1:01 - 2:21 a.m. on June 28, 1999, with only positrons circulating in the DAΦNE main rings, as reported by the DAΦNE beam monitor [21]. b) Observed number of clusters per half-CCD per minute (filled circles) during the corresponding beam period. The shaded area shows the results of the DEAR Monte Carlo simulation. The deviation of the first point is attributed to a high CCD occupancy [24].

Figure 2b and figure 3b show the number of clusters per half-CCD per minute observed with electron beams circulating in DAΦNE. The time dependence is given in correlation with the injection time of the beam into the accelerator ring. The time between two adjacent data points represents the exposure time (readout time) of the CCDs, which was 10 minutes.

10

The time behaviour of the number of clusters follows the time behaviour of the injected electrons, as given by the DAΦNE beam monitor [21] (reported in figures 2a and 3a). However, the observed time constant of the clusters' behaviour τ_c is actually different from the beam lifetime τ. Indeed, as a general rule deduced from the experimental data, it turns out that, for the various analyzed beam periods, τ_c is smaller than τ by a factor 1.2 - 2.0.
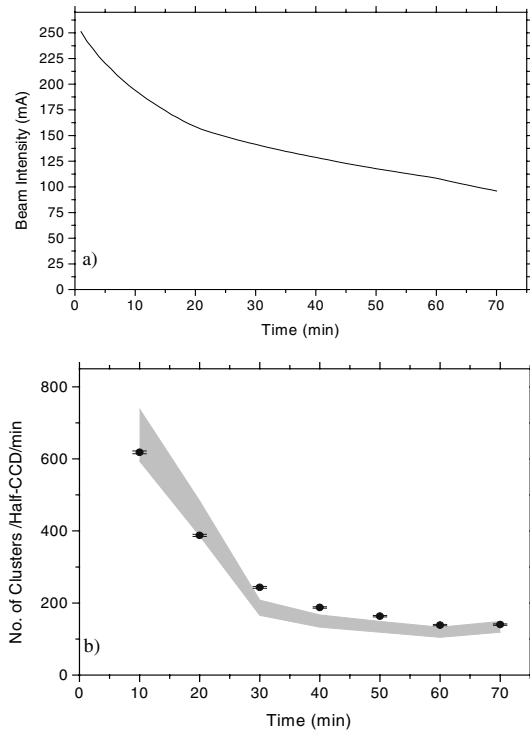
Figure 5: a) Positron beam intensity for the period 3:21 - 4:31 a.m. on June 28, 1999, with only positrons circulating in the DAΦNE main rings, as reported by the DAΦNE beam monitor [21]. b) Observed number of clusters per half-CCD per minute (filled circles) during the corresponding beam period. The shaded area shows the results of the DEAR Monte Carlo simulation.

An investigation similar to that done for electron beams was undertaken in the case of only positrons circulating in the DAΦNE main rings. The corresponding results of the number of clusters per half-CCD per minute are reported together with the respective beam intensities in figures 4 and 5 and compared with the simulations. The simulations agree with the measurements, although the agreement is not as good as for electron beams. In particular, the simulation slightly underestimates systematically the measured values of background and, therefore, the effective beam losses. This can probably be ascribed to the fact that the present situation of optimizing the machine towards higher luminosity is

not fully described by the Monte Carlo. In fact, the two beams are maintained separated in the interaction region where collisions do not occur, i.e. on the DEAR side, and shifted in opposite directions with respect to the magnetic axis, also when they circulate alone. Now it happens that the positron orbit is slightly more shifted than the electron one, a fact that is not taken into account by the Monte Carlo simulation. Due to the above mentioned characteristics of the Touschek effect this increases positron losses. Indeed, in the observed beam periods the positron beam lifetime was shorter than that for electron beams.
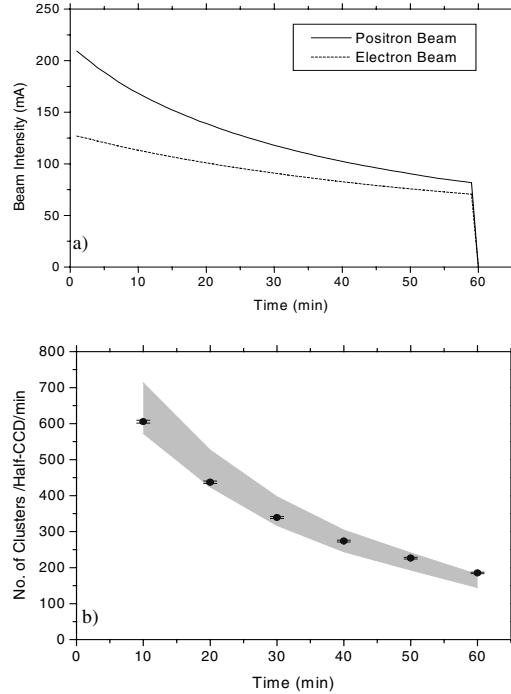
Figure 6: a) Beam intensities for simultaneously circulating electron and positron beams, separated in the DEAR interaction region, as reported by the DAΦNE beam monitor [21] for the period 7:31 - 8:31 p.m. on June 27, 1999. b) Observed number of clusters per half-CCD per minute (filled circles) during the corresponding beam period. The shaded area shows the results of the DEAR Monte Carlo simulation.

The deviation from the simulation in the first data point of Figs. 4b is caused by a general effect of CCD saturation due to high beam losses shortly after beam injection for the cases of poor injection efficiency. This high beam losses are reflected in a high CCD occupancy. A higher absolute number of clusters per CCD "image" enhances the probability that actually different clusters are located as neighbouring clusters. They are therefore indistinguishable for our analysis routines and counted as one cluster only [24]. This

saturation effect decreases therefore the measured background rate (number of clusters), and, consequently, the simulation overestimates in this case the rate. The unpredictable behaviour of the machine concerning the injection efficiency could obviously not be taken into account by the simulation.

In figure 5b, which reports a beam period just following that one reported in Fig. 4b, no deviation of the first data point from the simulation is apparent. This might be ascribed to an improvement of the injection efficiency which caused reduced beam losses compared to the previous beam period.
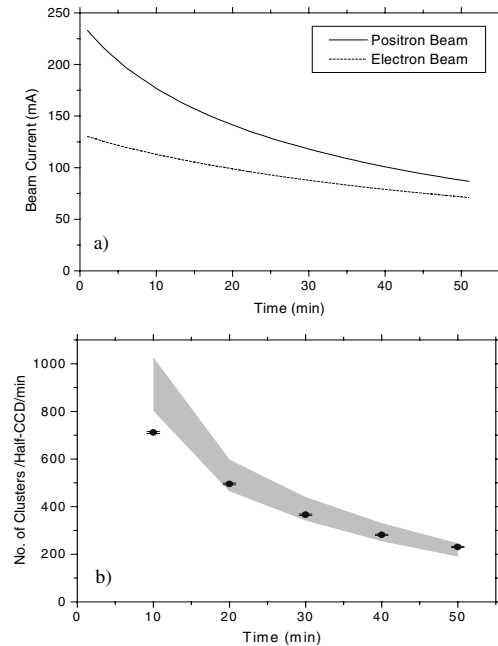
Figure 7: a) Beam intensities for simultaneously circulating electron and positron beams, separated in the DEAR interaction region, as reported by the DAΦNE beam monitor [21] for the period 10:01 - 10:51 p.m. on June 27, 1999. b) Observed number of clusters per half-CCD per minute (filled circles) during the corresponding beam period. The shaded area shows the results of the DEAR Monte Carlo simulation. The deviation of the first data point is attributed to a high CCD occupancy [24].

Finally, the background induced by two beams, electrons and positrons, circulating at the same time in the DAΦNE rings, but both being geometrically separated in the DEAR interaction region, is reported in figures 6b and 7b and compared with the corresponding simulations. The corresponding beam intensities are displayed in figures 6a and 7a for electrons and positrons. These measurements are also well reproduced by the Monte Carlo simulations. The deviation of the first data point in Fig. 7b must again be ascribed to CCD saturation due to high beam losses caused by a poor injection efficiency.

13

All measurements described in this paper took advantage of heavy shielding of the setup and were well reproduced by the simulation. In order to fully test the Monte Carlo routines, measurements without shielding were also performed.
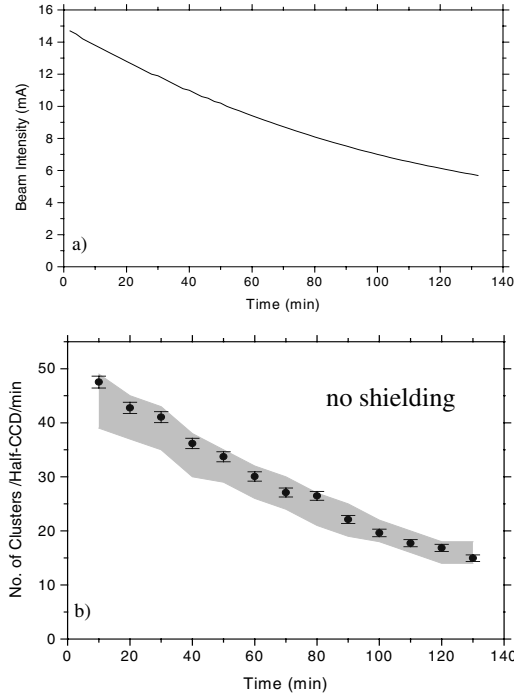
Figure 8: a) Electron beam intensity for the period 3:19 - 5:29 a.m. on April 22, 1999, with only electrons circulating in the DAΦNE main rings, as reported by the DAΦNE beam monitor [21]. b) Observed number of clusters per half-CCD per minute (filled dots) during the corresponding beam period measured with the unshielded setup. The shaded area shows the results of the DEAR Monte Carlo simulation.

Experimental and simulated results for a measurement without shielding are presented in figure 8. Again, the agreement is good. A shielding factor of 3.8 ± 0.4 can be extracted from the simulation for the adopted shielding configuration. Moreover, as result of the simulation, it turns out that ∼ 60 % of the shielding effect is obtained by shielding the bottom of the target cell, i.e. by the material placed between the target and the beam pipe.

The shielding factor can be directly measured. To do this, it is useful to introduce

the quantity ABCD (added beam current difference) (mA), defined as:

$$\mathrm{ABCD(mA)} = \sum_{e^-,e^+} I(t_0) - I(t_0 + t_M) \tag{1}$$

where $I(t_0)$ = beam intensity [21] at the time of the start of a CCD measurement, $I(t_0+t_M)$ = beam intensity [21] at the time of the stop of a CCD measurement, t_M = measurement time.
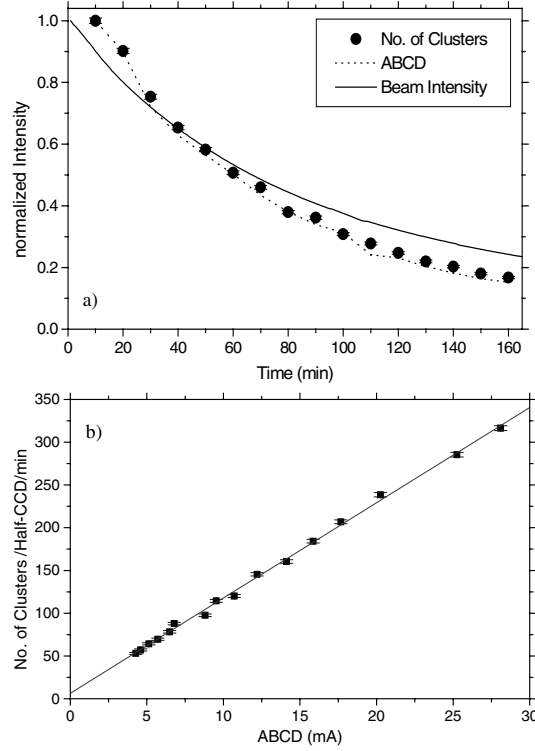
Figure 9: a) The time dependence of the number of clusters (filled circles) is given for the electron beam period 6:21 - 9:01 a.m. on June 27, 1999, in comparison with the quantity ABCD (dotted line) parametrizing the beam losses, and the beam intensity (full line), as reported by the DAΦNE beam monitor [21]. The maximum bin of all given quantitites is normalized to 1 to facilitate the comparison. b) ABCD dependence of observed number of clusters per half-CCD per minute for the same beam period (filled squares), together with a linear fit (line). See text for the definition of ABCD.

ABCD allows us to normalize, and therefore compare, beams with different initial intensities and different lifetimes. This quantity reflects the beam losses: since the number of clusters registered by CCD detectors (Clu) measures actually the particles lost from the beams, the added beam current difference and the clusters' number must have an identical

time behaviour, i.e. must have the same time constant, equal to τ_c. This is nicely shown in figure 9a, which shows as well the steeper time behaviour of the numbers of clusters with respect to the beam intensity ($\tau_c < \tau$).

The fact that ABCD and Clu have the same time constant is demonstrated by a linear dependence between these two quantities, as it is shown in Fig. 9b. Consequently, for each measurement in a given beam period - and therefore for any beam period - the number of registered clusters per beam losses (Clu/ABCD) during the corresponding time interval, is a constant. It can then be used as the parameter which characterizes a given beam period, independently of the initial intensity and of the lifetime. This is clearly shown in figure 10 which displays two examples of normalized numbers of clusters in different beam periods. The normalized numbers of clusters - one refers to electrons, the other to positrons - remain constant during the considered beam periods, a circumstance still valid for various investigated beam periods regarding both electrons and positrons. In these examples, positrons exhibit higher losses with respect to electrons, for the reasons discussed in relation to Figs. 4 and 5.
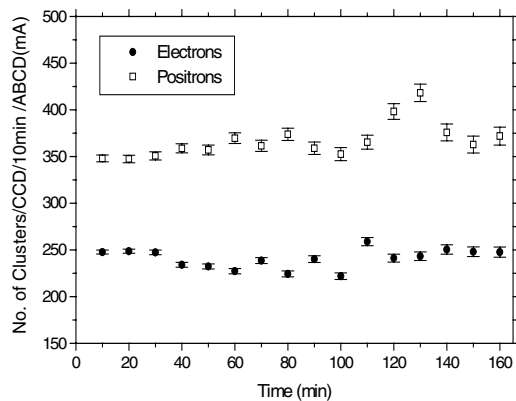
Figure 10: Time dependence of the ratio of the number of clusters per CCD per 10 minutes divided by the added beam current difference (ABCD) for two beams: electron beam on June 27 (filled circles) and positron beam on June 1 (open squares). The time behaviours are approximately constant. The rate of positron beam losses is higher than the electron one, as a consequence of the Touschek effect on particles circulating on an orbit slightly more shifted than the electron one with respect to the central ring axis (see text).

In table 1 the measured values of the ratio - number of Clusters per CCD per 10 minutes divided by ABCD - are given for several observed beam periods. The weighted mean values (wMean) for the observed beams of electrons only, positrons only, and electrons and positrons at the same time are given for the shielded and the unshielded setup in table 2.

16

Table 1: Ratio of the number of X rays/keV in the region of interest (BGX_{ROI}) divided by the number of clusters (Clu) in the case of unshielded and shielded setup for different types of beams. Integrated beam current (IBC) (mA$\times$h) calculated from the values reported by the DAΦNE beam monitor [21]. Measured values for the number of clusters per CCD per 10 minutes (Clu) divided by ABCD (defined in text).

Date	Beam type	IBC [mA$\times$h]	BGX_{ROI}/Clu $\times 10^{-4}$	Clu / ABCD (mA)
no shielding				
16.4.	$e^+ + e^-$	21.1	7.4 ± 0.7	——
19.4.	$e^+ + e^-$	13.6	7.1 ± 0.9	1010 ± 92
20.4.	e^-	19.5	8.0 ± 0.9	762 ± 120
22.4.	e^-	20.2	8.5 ± 1.0	828 ± 37
23.4.	$e^+ + e^-$	8.7	8.7 ± 0.8	1124 ± 235
shielding				
10.5.	$e^+ + e^-$	80.8	7.7 ± 0.7	——
11.5.	$e^+ + e^-$	61.4	6.0 ± 0.9	407 ± 100
17.5. P1	$e^+ + e^-$	161.7	8.5 ± 0.7	253 ± 17
17.5. P2	$e^+ + e^-$	187.0	7.5 ± 0.7	267 ± 12
18.5.	$e^+ + e^-$	293.3	6.3 ± 0.8	282 ± 19
1.6.	e^+	286.3	7.2 ± 0.7	361 ± 56
6.6.	e^-	154.5	9.0 ± 1.0	224 ± 13
27.6. P1	$e^+ + e^-$	213.7	6.3 ± 0.9	316 ± 50
27.6. P2	$e^+ + e^-$	192.3	7.3 ± 0.9	227 ± 11
27.6.	e^-	358.1	7.4 ± 0.8	241 ± 10
28.6. P1	e^+	183.8	7.9 ± 0.8	297 ± 15
28.6. P2	e^+	165.7	7.1 ± 0.8	294 ± 15
17.7.	$e^+ + e^-$	175.6	7.4 ± 0.8	——
Mean value			7.5 ± 0.5	see Tab.2

An explanation for the higher background with positrons was already given above. The value of the ratio Clu/ABCD measured with electrons and positrons in the interaction region at the same time, but geometrically separated (wMean(e^+e^-) = 253 $\pm$ 7), turns out to be equal to the weighted mean of the values measured with e^+ and e^- beams only, namely wMean((e^+)+(e^-)) = 257 $\pm$ 7. This shows that the contributions to the background simply add up for the two types of beam.

Finally, taking advantage of the possibility to normalize the number of clusters observed in different beam periods through the quantity ABCD, one can compare the background measured in the shielded setup with that registered in the unshielded configuration and deduce the effective shielding factor. This comparison is made in table 2, and figure 11

17

Table 2: Calculated weighted means (wMean) for the ratios of the number of clusters per CCD per 10 minutes (Clu) divided by ABCD (last column of table 1) for electron beams, positron beams, and electron and positron beams at the same time, for the shielded and the unshielded setup. Average shielding factors extracted from the weighted means and mean effective shielding factor.

wMean	Clu/ABCD (e^-)	Clu/ABCD (e^+e^-)	Clu/ABCD (e^+)
no shielding	822 ± 36	1025 ± 86	——
shielding	235 ± 8	253 ± 7	298 ± 11
average shielding factor	3.50 ± 0.20	4.05 ± 0.40	——
mean effective shielding factor	3.63 ± 0.20		——

shows a specific example. The higher background registered when the setup is not shielded is evident. The corresponding values for the shielding factor are given in table 2 for the two types of measurement, with electron beams only, and with electrons and positrons circulating at the same time. No beams of positrons only were available for a sufficiently long period, so no 'positrons only' measurements could be performed with the unshielded setup.
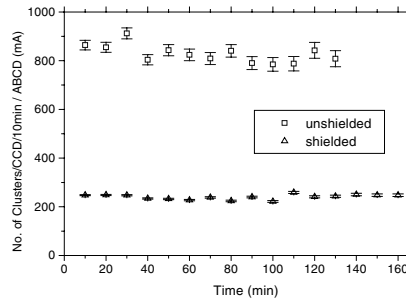
Figure 11: Time dependence of the normalized (by ABCD) numbers of clusters per CCD per 10 minutes from the electron beam on June 27, 1999 in the shielded setup (open triangles), and from April 22, 1999 in the unshielded setup (open squares). A shielding factor equal to 3.4 ± 0.3 can be derived from this specific data set.

From the two values for the effective shielding factor measured with the two types of beam, which agree within the errors, the weighted mean value for the measured effective shielding factor was derived to be equal to 3.6 ± 0.2, in agreement with the result of the simulation, i.e. 3.8 ± 0.4 .

18

5.1.3 Distribution of cluster sizes

The distribution of cluster sizes was also investigated. In the above mentioned preliminary background studies with only a single CCD detector set in a position asymmetric with respect to the interaction point a different cluster size distribution for electron and positron beams was found [23]. This was explained as a geometric effect associated with the type of beam (electrons or positrons). Since for the present measurements the CCD detectors were placed in a symmetric position, no difference was expected.

Normalization of the observed events for a specific cluster size to the total observed number of clusters allows to assign the probability to observe an event of this specific cluster size. Figure 12 shows these probabilities for various cluster sizes for the examples of e^-, e^+, and $e^- + e^+$ beams.
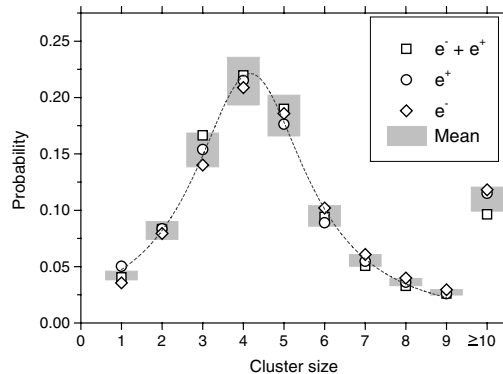
Figure 12: The measured probabilities for observing a hit with specific cluster size are given for three observed beams: electron beam (July 17, open diamonds), positron beam (June 28, open circles), electron and positron beam (May 18, open squares). The shaded area displays the mean value of the three measurements with a 10 % error. The dashed line displays a fit with a Lorentzian function.

The distribution can be fitted with a Lorentzian function with mean = 4.2 and width = 3.4 . All clusters with sizes larger than 9 were summed up in bin 10.

Within a 10 % error, cluster sizes induced by electron and positron beams are equally distributed. The maximum of all distributions have a peak at a cluster size equal to 4. This is related to the average charge deposited by a minimum ionizing particle in the substrate of the CCD chip.

19

5.2 X-ray observation

The goal of the DEAR experiment is to detect kaonic hydrogen X rays, therefore the study of the x-ray background is very important, particularly as the final statistical accuracy attainable with DEAR will critically depend on the level of x-ray background.

5.2.1 Background X rays

The energy of the kaonic hydrogen K_α peak is expected to be around 6 keV. Following the recent KEK result [4] the region of interest (ROI) for the DEAR experiment was selected to be 6.15 ± 0.6 keV. The full detection range of the CCD detector was selected to be 0.82 (1.0) keV up to 16.5 keV for the reported background measurements.

Two observed x-ray energy spectra are given in figure 13. Figure 13a) shows the result of ~ 2 weeks of measurements with circulating electron and positron beams with the unshielded setup and Ti and Zr foils inside the chamber. From both materials the electronic K_α lines can be clearly seen, and for Ti also the electronic K_β transition. This allows an online energy scale calibration. Additionally, the fluorescence lines of aluminum, of which both target and detector housings are made, and silicon, the material of the CCD chips, are visible. No line structure can be seen in the region of interest. In particular it should be mentioned that no structures at the energies of the electronic x-ray transitions originating from manganese and iron - materials present in normally available aluminum alloys - are present. This demonstrates the high purity of the aluminum selected for each component of the setup. Figure 13b) shows an energy spectrum taken for an equivalent period of time with the shielded setup and after removal of the Ti foils. The *K* lines from titanium ($K_\alpha = 4.5$ keV, $K_\beta = 4.9$ keV) would disruptingly interfere with the kaonic nitrogen $7 \to 6$ transition (~ 4.5 keV). The effect of shielding can be seen mainly by looking at the fluorescence lines of aluminum and silicon, which show a better separation against the smooth background. The spectrum of Fig.13b) was obtained after decreasing the low energy threshold. At this lower energy threshold one can already see the background increasing exponentially, because one starts to see the highest energy region of the "noise peak" of the CCDs, which is mainly caused by electronic noise [13].

The behaviour of soft X rays (≤ 20 keV) was also investigated as a function of time. The contribution of non-machine background to the given number of X rays per keV was measured to be negligible [23]. A behaviour identical to that observed for clusters should be, in principle, expected, since both clusters and X rays are produced by the e.m. cascades originated by the particles lost by the circulating beams and hitting the beam pipe and the setup materials. This expectation can be tested by determining the time behaviour of the ratio, number of X rays divided by number of clusters, which should then be constant.
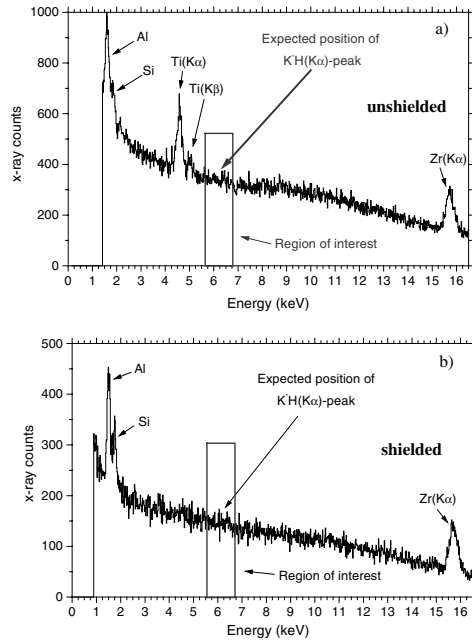
Figure 13: a) X-ray energy spectrum observed in ∼ 2 weeks with circulating electron and positron beams with the unshielded setup and Ti and Zr calibration foils. b) X-ray energy spectrum observed in ∼ 2 weeks with the shielded setup. In this measurement the Ti foils were removed and additional Zr foils attached. Both spectra show the expected fluorescence lines, while no significant structure can be observed in the region of interest, demonstrating the high purity of the aluminum employed for the setup. In measurement b) the low-energy threshold of the detector was reduced so the high energy tail of the noise peak can already be seen. Shielding yields a better separation of Al and Si lines against the background. However, a direct quantitative comparison of the two figures cannot be made because they were obtained with different total integrated beam currents.

Two regions characterize the energy spectrum: the region consisting of the energy intervals displaying the fluorescence lines of Si, Al and Zr (0.82 keV - 2.5 keV, 15.0 keV - 16.2 keV), and the region of the energy spectrum free of fluorescence lines, from 2.5 keV up to 15 keV, which contains the x-ray background created only by the particles lost by the beams. Additionally, we have selected the region which is of special interest for the DEAR experiment (ROI), from 5.55 keV up to 6.75 keV, where the kaonic hydrogen K_α peak is expected.

Figure 14 displays the ratio of the number of X rays per keV divided by the number of clusters for the two investigated energy regions as function of time. In this example, the $e^+ + e^-$ beams of May 18, 1999 were used. No deviation from a constant ratio can

be observed over the full energy interval from 2.5 keV up to 15 keV (Fig. 14a), which includes the region of interest (see inset). The same is true for the intervals where the fluorescence lines are present. In this case, the value of the ratio X rays per keV / clusters, is, as expected, larger (Fig.14b).

On the basis of the good agreement found between the number of measured clusters and the DEAR Monte Carlo simulation for different types of beams and periods of measurement, the measured constant value of the ratio X rays/clusters allows to make a quantitative determination of the expected x-ray background for the DEAR experiment. In table 1, the results for the ratio of the number of X rays per keV in the region of interest (BGX_{ROI}) divided by the number of clusters (Clu), obtained in different beam periods, both for the unshielded and for the shielded configuration, are listed. The ratio seems to be constant for both, shielded and unshielded configuration. The mean value of this ratio over all the measurements turns out to be $(7.5 \pm 0.5) \times 10^{-4}$.

The same value within errors was measured with the 2-CCD setup without any target cell and with the detector located in a quite different location of the DEAR interaction region still in the "Day-One" magnet configuration [25,23]. It can be concluded that this ratio reflects the beam background in the DEAR interaction region in the investigated period and does not depend on the specific setup used. A different type of background with a different energy and particle spectrum, e.g. non-machine background, results in a different value, i.e. $(0.1 \pm 0.05) \times 10^{-4}$, for the ratio X rays per keV in the region of interest divided by the number of clusters.

5.2.2 Fluorescence X rays

Using the energy spectra shown in figure 13 the following quantities can be determined:
- the number of X rays (X_i^{Peak}) observed in the fluorescence peaks of the materials (i = aluminum, titanium or zirconium) normalized to a surface of 1 cm^2 of the respective material;
- the number of X rays in the background below the respective peak (BG_i);
- the number of X rays in the region of interest for the experiment (BGX_{ROI});
- the ratio of the two quantities X_i^{Peak} / BG_i;
- the ratio of the two quantities X_i^{Peak} / BGX_{ROI}.
The obtained values for the two above defined peak-to-background ratios are given in table 3 for the shielded and for the unshielded setup.

The normalized number of X rays above background in the fluorescence peaks, found in the NTP target, can be used to obtain a first evaluation of the necessary surface of the calibration foils in the final cryogenic setup, in the sense of obtaining calibration peaks of

22
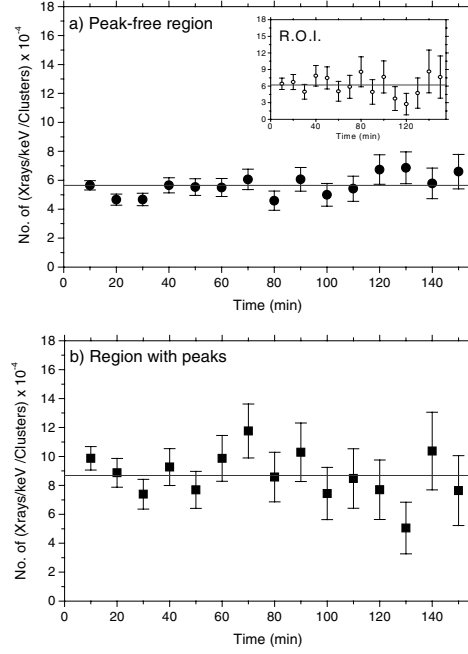
Figure 14: a) Measurement of the time behaviour of the ratios of the number of X rays per keV divided by the number of clusters, in the fluorescence-free energy region (2.5 keV - 15 keV), together with a linear fit (line); in the inset, the same is shown for X rays within the region of interest for the experiment, 5.55 keV - 6.75 keV. b) the same as in a) for the energy region consisting of the intervals where additional X rays from fluorescence peaks (Al, Si, Zr) are present, together with a linear fit (line).

comparable height with respect to that of the K_α signal. In the final configuration of the cryogenic setup, which will measure initially kaonic hydrogen, the signal/background ratio in the region of interest is about 2:1 [2]. From table 3 it turns out that, for instance for the zirconium line, a peak/background ratio of ~ 2, i.e. comparable with the signal/background ratio, could be reached with an overall surface of about 2000 cm^2.

The probability (per observed cluster and per cm^2 of material surface) to observe an electronic X ray excited in an attached calibration foil with a given surface area or in the target cell material is defined as:

$$P(X_i^{Exc})/cluster = \frac{X_i^{Peak}}{Clu} \, , \tag{2}$$

where X_i^{Peak} is the number of X rays / cm^2 observed in the fluorescence lines of the respective material (i = Al, Ti, Zr) and Clu is the observed number of clusters.

Table 3: Ratios of the number of fluorescence X rays per cm^2 (X_i^{Peak}) to the number of background X rays below the respective peak BG$_i$ and ratios of the number of fluorescence X rays per cm^2 (X_i^{Peak}) to the number of background X rays / keV in the region of interest (BGX$_{ROI}$), as obtained from the energy spectra shown in Fig.13

Peak i	Energy [keV]	X_i^{Peak} / BG$_i$ $\times 10^{-6}$	X_i^{Peak} / BG$_i$ $\times 10^{-6}$	X_i^{Peak} / BGX$_{ROI}$ $\times 10^{-6}$	X_i^{Peak} / BGX$_{ROI}$ $\times 10^{-6}$
		shielding	no shielding	shielding	no shielding
Al	1.5	117 ± 5	79 ± 4	58 ± 4	53 ± 4
Ti	4.5	——	333 ± 30	——	196 ± 8
Zr	15.7	969 ± 55	984 ± 80	288 ± 14	301 ± 12

Table 4: P(X_i^{Exc}) / cluster, the excitation probability for a fluorescence X ray per cm^2 per cluster for a specific material.

K$_\alpha$ peaks i	P(X_i^{Exc}) / cluster $\times 10^{-9}$	P(X_i^{Exc}) / cluster $\times 10^{-9}$
	shielding	no shielding
Al	43 ± 4	40 ± 4
Ti	——	147 ± 13
Zr	216 ± 18	226 ± 19

P(X_i^{Exc}) / cluster can be calculated by the following equation:

$$P(X_i^{Exc})/cluster = \frac{BGX_{ROI}}{Clu} \times \frac{X_i^{Peak}}{BGX_{ROI}} \,. \tag{3}$$

The value of the first factor is reported as mean value in table 1. The values of the second factor have been determined from the energy spectra of Fig. 13 and are reported in table 3. The resulting values for the probability per cm^2 per cluster to excite fluorescence X rays in the given materials are reported in table 4. These values are used as input parameters in the DEAR Monte Carlo simulation to obtain the final optimization of the experimental setup with respect to the surface of the calibration foils, in order to obtain the requested statistics in the corresponding peaks.

One can additionally compare, as a check, the measured relative fluorescence-peak ratios (Zr/Al, Zr/Ti, Ti/Al) with the corresponding ratios from literature [29]. In order to do this, it is necessary to introduce a correction factor, which takes into account the energy dependence both of the x-ray detection efficiency and of the machine background particles.

24

Table 5: Ratios of relative excitation probabilities for various observed fluorescence peaks $P(X_i^{Exc})/P(X_k^{Exc})$ compared to the ones derived from the tabulated values P_i^{Tab}/P_k^{Tab} [29]. The correction factors CF correspond to the evaluated background x-ray ratios BG_i/BG_k.

Ratio of K_α peaks i / k	CF	$P(X_i^{Exc})$ / $P(X_k^{Exc})$ $\times$ CF	CF	$P(X_i^{Exc})$ / $P(X_k^{Exc})$ $\times$ CF	P_i^{Tab} / P_k^{Tab}
i / k	shielding		no shielding		tabulation
Zr/Al	4.2 ± 0.2	20.9 ± 2.8	4.7 ± 0.2	26.7 ± 4.5	20.4 ± 1.8
Zr/Ti	——	——	2.6 ± 0.2	4.0 ± 0.6	3.3 ± 0.3
Ti/Al	——	——	1.8 ± 0.2	6.7 ± 1.2	6.1 ± 0.7

The correction factors arising from these effects, to be applied to the experimental relative fluorescence-excitation probabilities, are simply the ratios of the number of counts in the x-ray background under each fluorescence peak, already determined to obtain the peak/background ratios reported in table 3. The values of these correction factors (CF) are reported in table 5.

Using the probabilities $P(X_i^{Exc})$ / cluster reported in table 4 and these correction factors, the experimental relative fluorescence-excitation probabilities for the observed materials are obtained (table 5). They are compared with the ratios derived from the tabulated values in literature (table 5, last column). Significant quantitative agreement can be seen.

6   Summary

Measurements in the DEAR interaction region of the DAΦNE accelerator using the DEAR NTP setup were reported. These are the first measurements to be performed in this experimental area of the new electron-positron collider of Frascati National Laboratories. The background relevant for the DEAR experiment - low energy (≤ 20 keV) X rays and ionizing particles - in the presence of electron beams, positron beams, and both beams at the same time, but separated in the DEAR interaction region, was investigated.

The observed x-ray energy spectra do not show any evidence of unwanted structures. This demonstrates the purity of the construction materials used.

The number of x-ray events (single-pixel hits) and clusters (multi-pixel events), the latter corresponding to particles hitting the active area of the CCD detector, were observed. All measurements can be well reproduced by the DEAR Monte Carlo simulation using the actual beam parameters for the DEAR interaction region. With the present accelerator con-

figuration, the most important source of background comes from Touschek scattering, with a small contribution from beam-gas interaction. The quantitative agreement between simulation and measurements is sufficiently convincing to conclude that, with respect to the expected background, and, therefore, to the statistical error, the configuration which will be used for the measurement of the strong interaction shifts and widths in kaonic hydrogen and deuterium can obtain the planned challenging level of precision.

The improvement of the beam conditions up to their design values, additional lead wall shieldings on both sides of the target, and the use of beam scrapers to cut Touschek scattered particles before they are lost, promise that a larger reduction of the background for the DEAR experiment is yet possible.

Acknowledgements

References

[1] G. Vignola, *DAΦNE: the first Φ-Factory*, Proceedings of the "*5th European Particle Accelerator Conference (EPAC'96)*", Sitges (Barcelona), Eds. S. Myres *et al.*, Institute of Physics Publishing, Bristol and Philadelphia, 1996, p.22.

[2] S. Bianco et al., LNF-98/039 (P) (1998); Riv. del Nuovo Cimento 22, no.11 (1999) 1.

[3] J.D. Davies et al., Phys. Lett. 83B (1979) 55;
     M. Izycki et al., Z. Phys. A 297 (1980) 11;
     P.M. Bird et al., Nucl. Phys. A404 (1983) 482.

[4] T.M. Ito et al., Phys. Rev. A 58 (1998) 2366.

[5] T. Koike, T. Harada and Y. Akaishi, Phys. Rev. C53 (1996) 79.

[6] J. Zmeskal, unpublished.

[7] R. King, unpublished.

[8] B. Lauss et al., Phys. Rev. Lett. 80 (1998) 3041;
     B. Lauss et al., Phys. Rev. A 60 (1999) 209.

[9] B. Gartner et al., Hyperfine Interact. 101/102 (1996) 249.

[10] P. Hauser et al., Phys. Rev. C 58 (1998) R1869.

[11] D. Varidel et al., Nucl. Instr. and Meth. A 292 (1990) 141.

[12] G. Fiorucci et al., Nucl. Instr. and Meth. A 292 (1990) 147.

[13] J.-P. Egger, D. Chatellard, and E. Jeannet, Part. World 3 (1993) 139.

[14] D. Sigg, Nucl. Instr. and Meth. A 345 (1994) 107.

[15] R. Brun et al., GEANT3, CERN Report DD/EE/84-1 (1987).

[16] R. Baldini et al., LNF-95/055 (IR) (1995).

[17] S. Guiducci, Proceedings of the "*5th European Particle Accelerator Conference (EPAC'96)*", Sitges (Barcelona), Eds. S. Myres et al., Institute of Physics Publishing, Bristol and Philadelphia, 1996, p.1365.

[18] S. Guiducci, DAΦNE Technical Note IR-5 (June 15, 1994).

[19] S. Guiducci, DAΦNE Technical Note IR-6 (April 26, 1995).

[20] S. Guiducci and M.A. Iliescu, LNF-97/002 (IR) (1997).

[21] DAΦNE beam monitor, http://dafne.lnf.infn.it, DAΦNE divisione acceleratori, Laboratori Nazionali di Frascati dell'INFN, I-00044 Frascati, Italy.

[22] G. Fiorucci, Thesis, University of Neuchâtel, 1990, unpublished.

[23] B. Lauss et al., DEAR Technical Note IR-10 (March 26, 1999).

[24] B. Lauss, unpublished.

[25] M. Augsburger et al., DEAR Technical Note IR-9 (November 8, 1998).

[26] C. Petrascu, DEAR Technical Note IR-8 (November 2, 1998).

[27] C. Petrascu, DEAR Technical Note IR-12 (February 3, 1999).

[28] C. Petrascu, DEAR Technical Note IR-13 (June 16, 1999).

[29] W. Bambynek et al., Rev. Mod. Phys. 44 (1972) 716.

List of Figures

List of Tables